Hierarchical Self-Assembly on Silicon

ARTICLE *in* JOURNAL OF THE AMERICAN CHEMICAL SOCIETY · MARCH 2010

Impact Factor: 12.11 · DOI: 10.1021/ja9099938 · Source: PubMed

7 AUTHORS, INCLUDING:

Damiano Genovese
Karlsruhe Institute of Technology
31 PUBLICATIONS **500** CITATIONS
SEE PROFILE

Luigi Cristofolini
Università degli studi di Parma
95 PUBLICATIONS **788** CITATIONS
SEE PROFILE

Luca Prodi
University of Bologna
207 PUBLICATIONS **7,032** CITATIONS
SEE PROFILE

Enrico Dalcanale
Università degli studi di Parma
198 PUBLICATIONS **4,398** CITATIONS
SEE PROFILE

J|A|C|S
ARTICLES

Published on Web 03/10/2010

Hierarchical Self-Assembly on Silicon

Francesca Tancini,[†] Damiano Genovese,[‡] Marco Montalti,[‡] Luigi Cristofolini,[&] Lucia Nasi,[§] Luca Prodi,[‡] and Enrico Dalcanale*[,†]

Dipartimento di Chimica Organica e Industriale, Università di Parma, and INSTM UdR Parma, 43124 Parma, Italy, Dipartimento "G. Ciamician", Università di Bologna, 40126 Bologna, Italy, Dipartimento di Fisica, Università di Parma, 43124 Parma, Italy, and Istituto CNR-IMEM, 43124 Parma, Italy

Received November 25, 2009; E-mail: enrico.dalcanale@unipr.it

Abstract: A set of modular components was designed, synthesized, and combined to yield an innovative, robust, and reliable methodology for the self-assembly of large supramolecular structures on silicon wafers. Specific host−guest and H-bonding motifs were embedded in a single molecule by exploiting the remarkable complexing properties of tetraphosphonate cavitands toward methylammonium and methylpyridinium salts and the outstanding homo- and hetero-dimerization capability of the ureidopyrimidone moiety. An assembly/disassembly sequence in solution was devised to assess the orthogonality and reversibility of H-bonding and host−guest interactions. The entire process was fully tested and characterized in solution and then successfully transferred to the solid state. The selected binding motifs resulted to be fully compatible in the assembly mode and individually addressable in the disassembly mode. The complete orthogonality of the two interactions allows the molecular level control of each step of the solid-state assembly and the predictable response to precise external stimuli. Complementary surface analysis techniques, such as atomic force microscopy (AFM), ellipsometry, and fluorescence, provided the univocal characterization of the realized structures in the solid state.

Introduction

The development of self-assembly protocols generating functional surfaces with well-defined structures and tunable properties is one of the main goals of modern materials chemistry.[1] The perspective of hybrid materials, held together by different kinds of noncovalent interactions, presenting distinct and unrelated association dynamics, is particularly intriguing because they lead to adaptive materials,[2] characterized by switchable functions. The resulting complexity of these hybrid materials requires implementing combinations of two or more different interaction modes, among which hydrogen bonding, host−guest complexation, and metal−ligand coordination are pivotal. They have in common a high level of structural definition and tunable strength, which allow the design of functional materials at the molecular level. Although these weak interactions were employed individually to build supramolecular architectures on surfaces,[3−6] few efforts have been made on the route of their concurrent employment for the generation of hybrid materials and stimuli-responsive surfaces.[7−9]

Starting from this premise, we designed a set of molecules featuring one or two binding motifs, to use as "switching modules" to control the self-assembly process in the multistep growth of supramolecular structures on silicon. As binding motifs, we chose hydrogen bonding and host−guest interactions, because of their tunable strength, selectivity, and directionality. For H-bonding, we exploited the self-assembly of ureidopyrimidone (UPY) derivatives and 2,7-diamino-1,6-naphthyridine diamides (NAPY) to generate robust H-bonded heterodimers.[10]

[†] Dipartimento di Chimica Organica e Industriale, Università di Parma.
[‡] Dipartimento "G. Ciamician", Università di Bologna.
[&] Dipartimento di Fisica, Università di Parma.
[§] Istituto CNR-IMEM.

(1) Descalzo, A. B.; Martìnez-Màòez, R.; Sancenòn, F.; Hoffmann, K.; Rurack, K. *Angew. Chem., Int. Ed.* **2006**, *45*, 5924–5948.
(2) Lehn, J. M. *Chem.—Eur. J.* **1999**, *5*, 2455–2463.
(3) (a) H-bonding: De Feyter, S.; De Schryver, F. C. *Chem. Soc. Rev.* **2003**, *32*, 139–150. (b) Theobald, J. A.; Oxtoby, N. S.; Phillips, M. A.; Champness, N. R.; Beton, P. H. *Nature* **2003**, *424*, 1029–1031. (c) Ruben, M.; Payer, D.; Landa, A.; Comisso, A.; Gattinoni, C.; Lin, N.; Collin, J. P.; Sauvage, J.-P.; De Vita, A.; Kern, K. *J. Am. Chem. Soc.* **2006**, *128*, 15644–15651. (d) Llanes-Pallas, A.; Matena, M.; Jung, T.; Prato, M.; Stöhr, M.; Bonifazi, D. *Angew. Chem., Int. Ed.* **2008**, *47*, 7726–7730. (e) Madueno, R.; Räisänen, M. T.; Silien, C.; Buck, M. *Nature* **2008**, *454*, 618–621.
(4) (a) Host−guest: Ludden, M. J. W.; Reinhoudt, D. N.; Huskens, J. *Chem. Soc. Rev.* **2006**, *35*, 1122–1134. (b) Ludden, M. J. W.; Mulder, A.; Tampè, R.; Reinhoudt, D. N.; Huskens, J. *Angew. Chem., Int. Ed.* **2007**, *46*, 4104–4107.
(5) (a) Metal−ligand coordination: Weissbuch, I.; Baxter, P. N. W.; Cohen, S.; Cohen, H.; Kjaer, K.; Howes, P. B.; Als-Nielsen, J.; Hanan, G. S.; Schubert, U. S.; Lehn, J.-M.; Leiserowitz, L.; Lahav, M. *J. Am. Chem. Soc.* **1998**, *120*, 4850–4860. (b) Hatzor, A.; Moav, T.; Cohen, H.; Matlis, S.; Libman, J.; Vaskevich, A.; Shanzer, A.; Rubinstein, I. *J. Am. Chem. Soc.* **1998**, *120*, 13469–13477. (c) Levi, S.; Guatteri, P.; van Veggel, F. C. J. M.; Vancso, G. J.; Dalcanale, E.; Reinhoudt, D. N. *Angew. Chem., Int. Ed.* **2001**, *40*, 1892–1896. (d) Busi, M.; Laurenti, M.; Condorelli, G. G.; Motta, A.; Favazza, M.; Fragalà, I. L.; Montalti, M.; Prodi, L.; Dalcanale, E. *Chem.—Eur. J.* **2007**, *13*, 6891–6898. (e) Li, S.-S.; Northrop, B. H.; Yuan, Q.-H.; Wan, L.-J.; Stang, P. J. *Acc. Chem. Res.* **2009**, *42*, 249–259.
(6) π-Stacking: (a) Bhosale, R.; Perez-Velasco, A.; Ravikumar, V.; Kishore, R. S. K.; Kel, O.; Gomez-Casado, A.; Jonkheijm, P.; Huskens, J.; Maroni, P.; Borkovec, M.; Sawada, T.; Vauthey, E.; Sakai, N.; Matile, S. *Angew. Chem., Int. Ed.* **2009**, *48*, 6461–6464. (b) Kishore, R. S. K.; Kel, O.; Banerji, N.; Emery, D.; Bollot, G.; Mareda, J.; Gomez-Casado, A.; Jonkheijm, P.; Huskens, J.; Maroni, P.; Borkovec, M.; Vauthey, E.; Sakai, N.; Matile, S. *J. Am. Chem. Soc.* **2009**, *131*, 11106–11116.

Chart 1

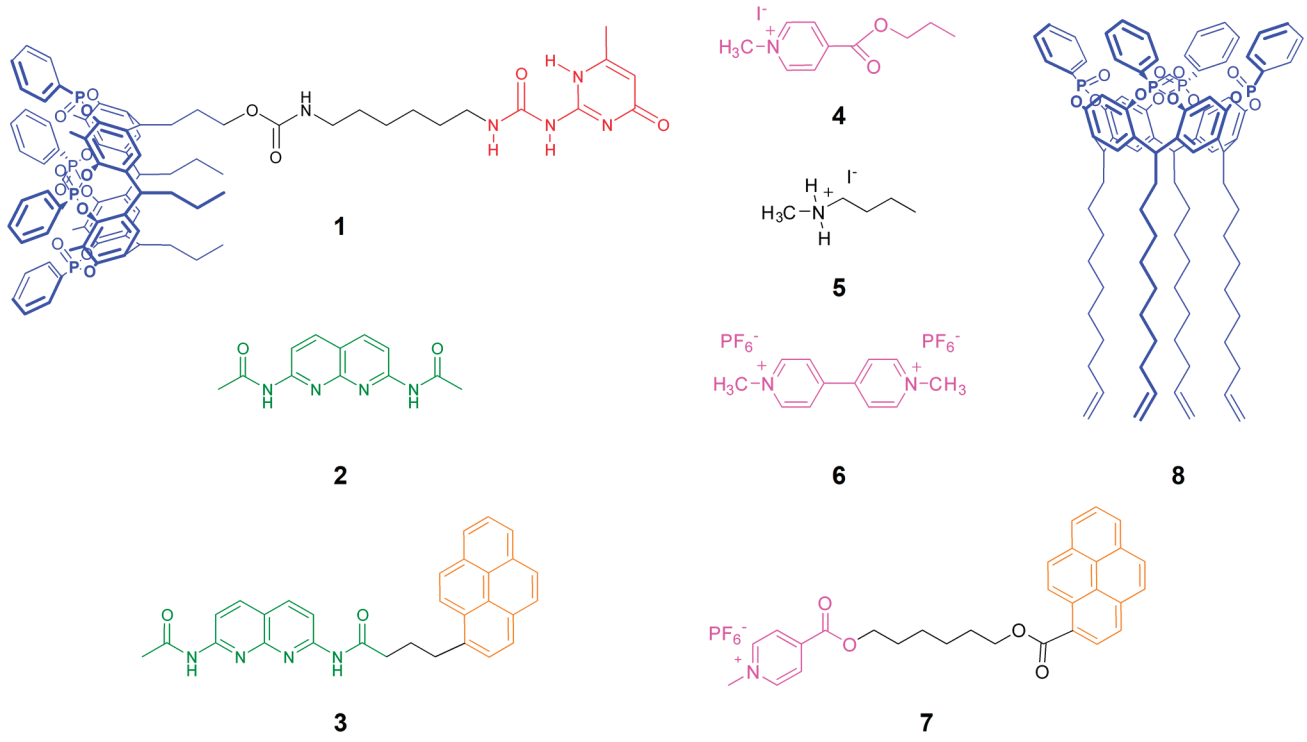

For the host−guest binding mode, our long-standing interest in phosphonate cavitand chemistry[11] led us to employ these molecules as efficient hosts for *N*-methylpyridinium and *N*-methylammonium salts.[12] The two have in common the following features: (i) remarkable stability of their respective complexes with K_{ass} above 10^7 M^{-1} in chlorinated solvents; (ii) high fidelity in recognition. The first characteristic is crucial for generating robust self-assembly protocols, while the second is essential for the orthogonality of the two interaction modes. An additional feature pertaining to the host−guest motif is the presence of specific decomplexation modes, operating either electrochemically[13] or via protonation/deprotonation.[12a] Silicon was chosen as inorganic surface, since it is a technologically relevant platform and it allows the formation of very stable and durable grafting via Si−C bonds.

In this paper we report a precise and reversible hierarchical assembly on silicon using a sequence of host−guest and H-bonding interactions. The entire process has been fully tested and characterized in solution, and then successfully transferred to the solid state. The complete orthogonality of the two interactions allows the molecular level control of each step of the solid-state assembly and the predictable response to precise external stimuli.

Results and Discussion

Synthesis of the Molecular Components. The compounds used in the present work are shown in Chart 1, and their preparation is reported in the Supporting Information (SI). The target molecule **1** was synthesized in five steps starting from the known monohydroxy-footed silylcavitand **I** (Scheme 1).[12b] The hydroxyl group at the lower rim was initially protected by reaction with chloromethyl methyl ether. The subsequent treatment of the resulting product **II** with an aqueous 36% HF solution caused the selective removal of the dimethylsilyl bridges, affording the free resorcinarene **III**, ready for the functionalization with dichlorophenylphosphine. This latter reaction gave rise to a tetraphosphonite intermediate,[14] which was *in situ* oxidized by addition of H_2O_2,[12b] to give tetraphosphonate cavitand **IV**. Only the isomer featuring all the P═O groups pointing toward the cavity was formed, due to the stereospecificity of this bridging reaction. Then, the methylmethoxy protection was removed by an HCl-catalyzed hydrolysis to give **V**. Addition of 2(6-

(7) Langner, A.; Tait, S. L.; Lin, N.; Chandrasekar, R.; Ruben, M.; Kern, K. *Angew. Chem., Int. Ed.* **2008**, *47*, 8835–8838.
(8) For alternative combinations of orthogonal interaction modes on surfaces, see: (a) Corbellino, F.; Mulder, A.; Sartori, A.; Ludden, M. J. W.; Casnati, A.; Ungaro, R.; Huskens, J.; Crego-Calamata, M.; Reinhoudt, D. N. *J. Am. Chem. Soc.* **2004**, *126*, 17050–17058. (b) Ludden, M. J. W.; Huskens, J.; Reinhoudt, D. N. *Small* **2006**, 1192–1202.
(9) For the combination of weak interactions in supramolecular polymers see: Hofmeier, H.; Schubert, U. S. *Chem. Commun.* **2005**, 2423–2432.
(10) (a) Beijer, F. H.; Sijbesma, R. P.; Kooijman, H.; Spek, A. L.; Meijer, E. W. *J. Am. Chem. Soc.* **1998**, *120*, 6761–6769. (b) Corbin, P S.; Zimmermann, S. C. *J. Am. Chem. Soc.* **1998**, *120*, 9710–9711. (c) Wang, X.-Z.; Li, X.-Q.; Shao, X.-B.; Zhao, X.; Deng, P.; Jiang, X.-K.; Li, Z.-T.; Chen, Y.-Q. *Chem.—Eur. J.* **2003**, *9*, 2904–2913. (d) Park, T.; Todd, E. M.; Nakashima, S.; Zimmermann, S. C. *J. Am. Chem. Soc.* **2005**, *127*, 18133–18142. (e) de Greef, T. F. A.; Ligthart, G. B. W. L.; Lutz, M.; Spek, A. L.; Meijer, E. W.; Sijbesma, R P. *J. Am. Chem. Soc.* **2008**, *130*, 5479–5486.
(11) (a) Pinalli, R.; Suman, M.; Dalcanale, E. *Eur. J. Org. Chem.* **2004**, 451–462. (b) Pirondini, L.; Dalcanale, E. *Chem. Soc. Rev.* **2007**, *36*, 695–706.
(12) (a) Biavardi, E.; Battistini, G.; Montalti, M.; Yebeutchou, R. M.; Prodi, L.; Dalcanale, E. *Chem. Commun.* **2008**, 1638–1640. (b) Yebeutchou, R. M.; Tancini, F.; Demitri, N.; Geremia, S.; Mendichi, R.; Dalcanale, E. *Angew. Chem., Int. Ed.* **2008**, *47*, 4504–4507. (c) Biavardi, E.; Favazza, M.; Motta, A.; Fragala, I. L.; Massera, C.; Prodi, L.; Montalti, M.; Melegari, M.; Condorelli, G.; Dalcanale, E. *J. Am. Chem. Soc.* **2009**, *131*, 7447–7455.
(13) Gadenne, B.; Semeraro, M.; Yebeutchou, R. M.; Tancini, F.; Pirondini, L.; Dalcanale, E.; Credi, A. *Chem.—Eur. J.* **2008**, *14*, 8964–8971.
(14) Xu, W.; Rourke, J. P.; Puddephatt, R. J. R. *Chem. Commun.* **1993**, 145–147.

Scheme 1[a]

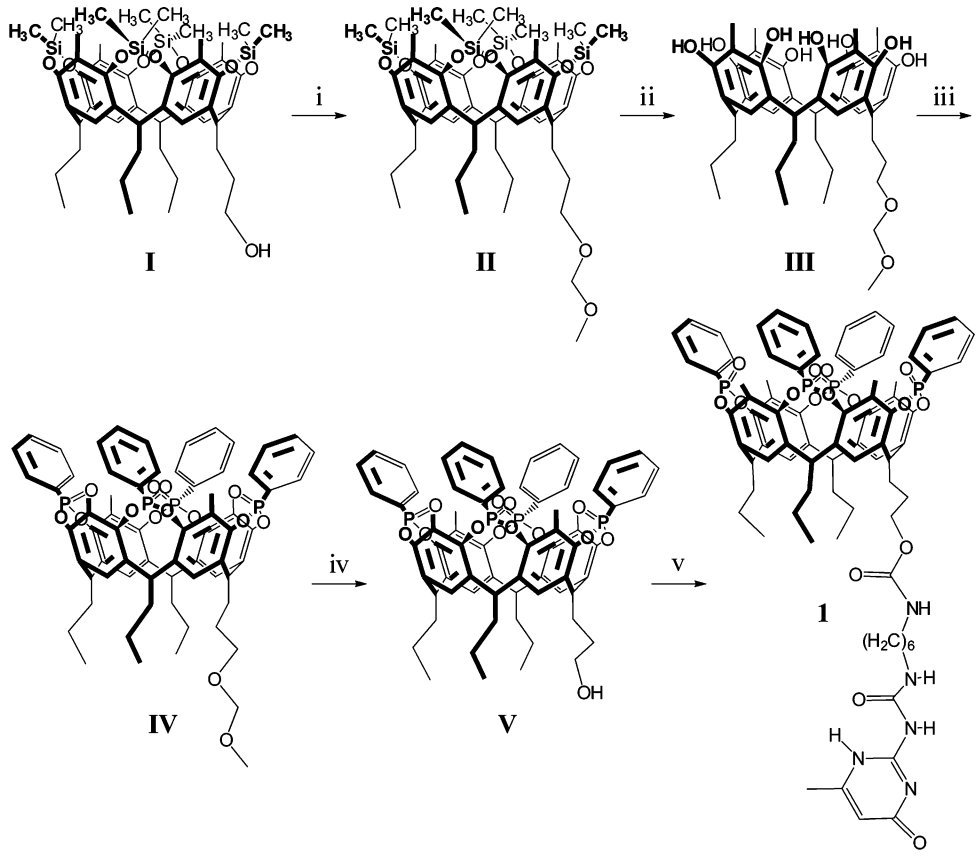

[a] (i) DIPA, $CHCl_3$/DMF, 40 °C, 48 h, 75%; (ii) HF, DMF, 45 °C, overnight, qt. yield; (iii) $PhPCl_2$, pyridine, 70 °C, 3 h; $H_2O_2/CHCl_3$, rt, 30 min, qt. yield; (iv) HCl, $CHCl_3$/MeOH, 60 °C, overnight, 93%; 2(6-isocyanatohexylaminocarbonylamino)-6-methyl-4[1]pyrimidinone, DABCO, $CHCl_3$, reflux, 48 h, 49%.

isocyanatohexylaminocarbonylamino)-6-methyl-4[1]pyrimidinone[15] at the free hydroxyl function, in the presence of 1,4-diazobicyclo[2.2.2]octane (DABCO) as catalyst, afforded cavitand **1** in 34% overall yield.

The symmetric 2,7-acetamido-1,8-naphthyridine **2** was prepared following a known literature protocol,[16] while the asymmetric 2(1-pyrenebutyricamido)-7-acetamido-1,8-naphthyridine **3** was synthesized by the Pd-catalyzed amidation of 2-chloro-7-acetamido-1,8-naphthyridine,[17] according to a procedure reported by Meijer and co-workers.[18]

Preparation of monotopic guests **4**, **5**, and **7** was previously reported,[12a] as well as that of cavitand **8**.[19]

Properties of the Modular Components 1 and 3. Cavitand **1** is functionalized at the upper rim with four phosphonate bridges in their all-inward configuration and at the lower rim with a single ureidopyrimidone (UPY) unit. While the P═O groups impart molecular recognition properties toward methylpyridinium guests and methylammonium salts, the UPY motif enables the molecule to dimerize according to a DDAA-AADD quadruple H-bonding network (A, D: hydrogen bond acceptor and donor, respectively). The association constant between a tetraphosphonate cavitand and a methylpyridinium guest was determined by ITC and fluorescence to be in the 10^7 M^{-1} regime (CH_2Cl_2, 298 K),[12a] while complexation of methylalkylammonium salts is much stronger, occurring with constants not directly measurable via ITC.[12b] As far as the UPY unit is conceYrned, Meijer and co-workers showed that DDAA-AADD sequences have a dimerization constant of 6×10^7 M^{-1} ($CHCl_3$, 298 K).[20]

The asymmetric 2,7-diamino-1,6-naphthyridine diamide (NAPY) **3** was equipped with a pyrenic unit to allow fluorescence monitoring of its complexation/decomplexation both in solution and on surfaces. Moreover, in addition to its homodimerization capability, which is quite weak (K_{ass}= 10^1-10^2 M^{-1}, $CHCl_3$, 298 K), **3** is complementary to an ADDA H-bonding array. This is the typical array shown by UPY systems, once the self-complementary 4[1H]-pyrimidinone conformer isomerizes to the noncomplementary 4[3H]-pyrimidinone conformer (Figure 1). For this reason NAPY motifs like that of molecule **3** are used to dissociate stable UPY−UPY homodimers and to turn them in robust UPY−NAPY heterodimers,[21] introducing switchability in H-bonded networks.

Molecules **4** and **6** are efficiently complexed by tetraphosphonate cavitands, thanks to a synergistic combination of multiple cation−dipole and $CH_3-\pi$ interactions.[12c] While guest

(15) Keizer, H. M.; Van Kessel, R.; Sijbesma, R. P.; Meijer, E. W. *Polymer* **2003**, *44*, 5505–5511.
(16) Alvarez-Rua, C.; Garcia-Granda, S.; Goswami, S.; Mukherjee, R.; Dey, S.; Claramunt, R. M.; Maria, M. D. S.; Rozas, I.; Jagerivic, N.; Alkorta, I.; Elguero, J. *New J. Chem.* **2004**, *28*, 700–707.
(17) Corbin, P. S.; Zimmerman, S. C.; Thiessen, P. A.; Hawriluk, N. A.; Murray, T. J. *J. Am. Chem. Soc.* **2001**, *123*, 10475–10488.
(18) Lightart, G. B. W. L.; Ohkawa, H.; Sijbesma, R. P.; Meijer, E. W. *J. Org. Chem.* **2006**, *71*, 375–378.
(19) Bibal, B.; Tinant, B.; Declercq, J.-P.; Dutasta, J.-P. *Supramol. Chem.* **2003**, *15*, 25–32.
(20) Sontjens, S. H. M.; Sijbesma, R. P.; Van Genderen, M. H. P.; Meijer, E. W. *J. Am. Chem. Soc.* **2000**, *122*, 7487–7493.
(21) (a) Zhao, X.; Wang, X.-Z.; Jiang, X.-K.; Chen, Y.-Q.; Li, Z.-T.; Chen, G.-J. *J. Am. Chem. Soc.* **2003**, *125*, 15128–15139. (b) Li, X.-Q.; Feng, D.-J.; Jiang, X.-K.; Li, Z.-T. *Tetrahedron* **2004**, *60*, 8275–8284.

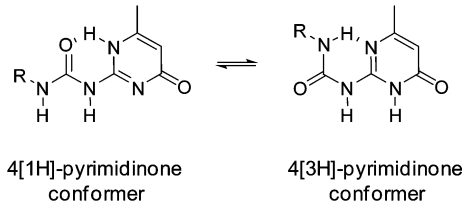

Figure 1. Pyrimidinone isomerization between 4[1H] and 4[3H] forms.

Scheme 2. Assembly/Disassembly Sequence in Solution

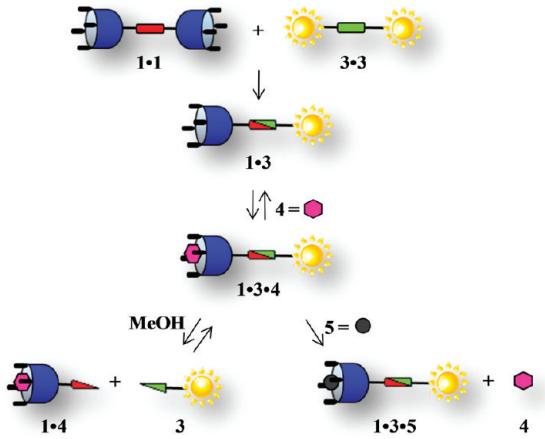

4 presents just one binding site, leading to the formation of 1:1 complexes, methylviologen **6** has a ditopic character, allowing formation of 2:1 complexes.[22] For this reason monotopic guest **4** was chosen for the complexation studies in solution, while ditopic guest **6** was employed to build supramolecular structures on the silicon surface. Finally, tetraphosphonate cavitands bind very efficiently methylalkylammonium salts such as *N*-methylbutylammonium iodide **5**. The additional, synergistic H-bonding interactions between the adjacent inward-facing P(O) groups and the two NH of the guest enhance the complexation. This results in a higher association constant for this guest family, which justifies the use of methylalkylammonium salts as effective competitive guests to replace methylpyridinium species.

Complexation Studies in Solution. In order to test the orthogonality and reversibility of H-bonding and host−guest interactions, we performed complexation studies in solution monitored by ^{1}H NMR spectroscopy.

The following sequential set of experiments was devised: (i) formation of **1·3** UPY·NAPY heterodimer; (ii) complexation of the monotopic methylpyridinium guest **4** by **1·3** to give the ternary complex **1·3·4**; (iii) selective disassembly/reassembly of the H-bond motif in **1·3·4**; (iv) guest exchange in **1·3·4** to give **1·3·5** using methylbutylammonium iodide **5**. The entire sequence is sketched in Scheme 2.

(i) UPY·NAPY Heterodimer Formation. In chloroform solution, monomers **1** and **3** exist exclusively as **1·1** and **3·3** homodimers, as confirmed by the presence, in the ^{1}H NMR spectrum, of signals typical for the hydrogen-bonded NH protons (red triangles in Figure 2a and green triangles in Figure 2b). Addition of increasing amounts of **3·3** to a **1·1** solution resulted in the complete dissociation of **3·3** and in the concurrent exclusive formation of **1·3** heterodimer. This process was proved by the disappearance of the NH signals related to the **3·3** H-bonded complex and by the appearance of two sets of

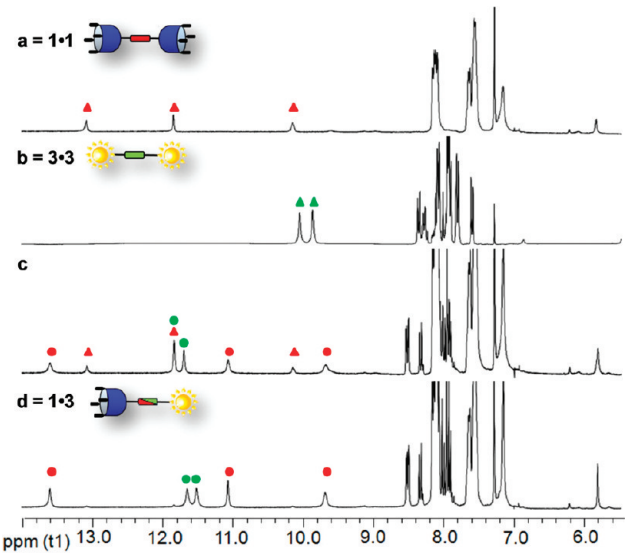

Figure 2. Section of ^{1}H NMR spectra (10 mM, $CDCl_3$) monitoring of UPY-NAPY **1·3** formation: diagnostic NH signals of (a) **1·1** (red triangles), (b) **3·3**, (green triangles), (c) **1·1** + **1·3** (1:0.5), and (d) **1·3** (red + green dots).

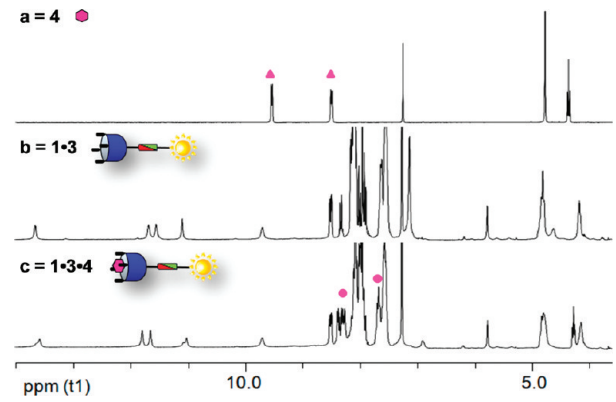

Figure 3. Section of ^{1}H NMR spectra (10 mM, $CDCl_3$) monitoring host−guest complexation: signals relative to N-Me pyridinium aromatic protons of (a) **4** (pink triangles), (b) **1·3** (1:1), and (c) **1·3·4** (1:1:1, pink dots).

NH signals due to the UPY NH protons. The first set, relative to the **1·1** homodimer, vanished when the 1:1 ratio was reached, meanwhile the second set increased in magnitude to become the only one present (red and green dots in Figures 2c and 2d). Moreover, a shift for the NAPY NH peaks was observed, consistent with a slow equilibration of dimers on the NMR experiment time scale.

(ii) Host−Guest Complexation. Addition of **4** gave rise to the hybrid H-bonded/host−guest system **1·3·4**. Formation of the host−guest complex was proved by the upfield shift of H_{ORTHO} and H_{META} pyridine protons, due to the shielding effect of the receptor cavity (spectra a and c in Figure 3). On the other hand, the unchanged position of H-bonded NH protons demonstrated that host−guest complex formation did not interfere with the previously assembled UPY−NAPY dimer (spectra b and c in Figure 3).

(iii) H-Bonding Motif Disassembly/Reassembly. Addition of MeOD to the **1·3·4** solution ($CDCl_3$/MeOD, 8:2) produced the selective disassembly of the H-bonded heterodimer, while the host−guest system persisted (see SI, spectrum b in Figure S1). When the added MeOD was removed by vacuum evaporation

(22) Dutasta, J.-P.; et al. *Phosphorus, Sulfur Silicon* **2002**, *177*, 1485–1488.

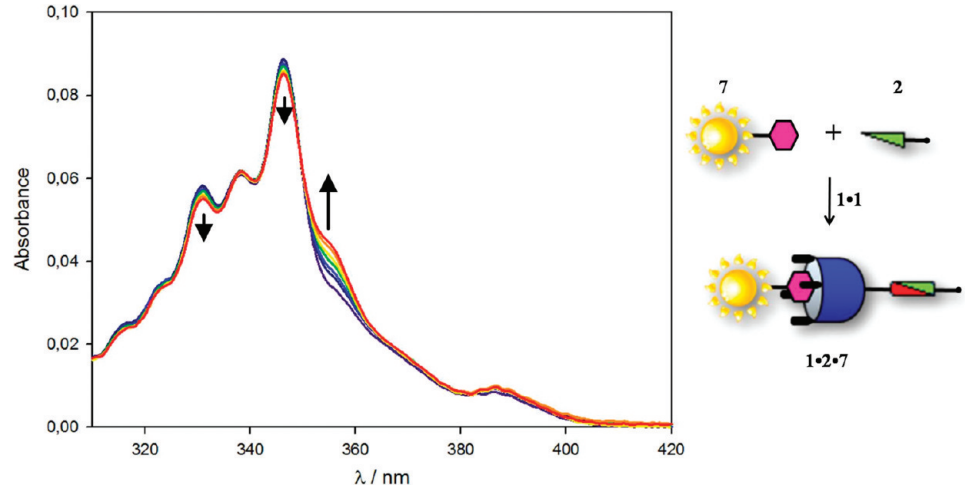

Figure 4. Absorption spectra of a 2×10^{-6} M solution of **2** and **7** and upon addition of an increasing amount of **1** (0−1 equiv).

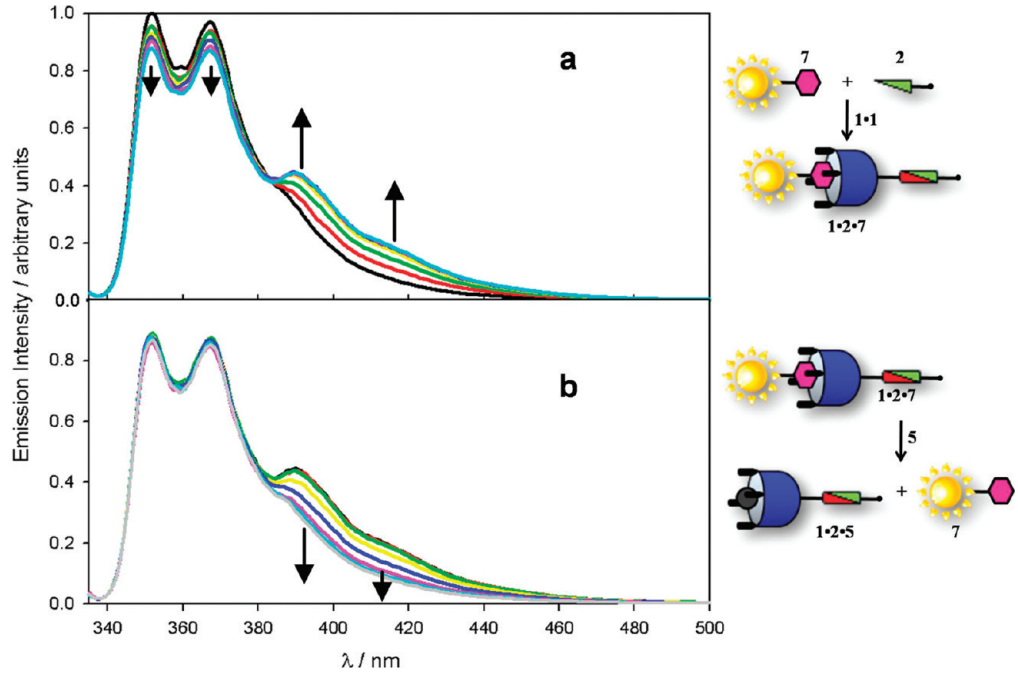

Figure 5. Emission spectra ($\lambda_{exc} = 325$ nm) of a 2×10^{-6} M solution of **2** and **7** and upon addition of an increasing amount of **1** (0−1 equiv) (a) and upon subsequent addition of **5** (0−1 equiv) (b).

and the sample was redissolved in $CDCl_3$, the initial **1·3·4** ternary complex was fully restored, demonstrating the solvent-dependent reversibility of the H-bond motif (see SI, spectra a and c in Figure S1).

(iv) Guest Exchange. Addition of 1 equiv of **5** to the **1·3·4** complex led to the formation of the new **1·3·5** ternary complex. The position of the aromatic pyridine protons and the upfield shifts undergone by the NH and N−CH_3 of the ammonium salt proved that the competitive guest replaced completely the methylpyridinium moiety inside the cavity (see SI, spectrum d in Figure S2). This process again did not interfere with the **1·3** heterodimer, as demonstrated by the unchanged position of the H-bonded NH signals.

Fluorescence Complexation Studies in Solution. The above findings were also supported by photophysical investigations. In this case, the three-component assembly was proved by starting from an equimolar solution (2×10^{-6} M) of **2** and **7**, which presents a methylpyridinium unit as recognition moiety connected to a pyrene unit. This latter system was used in this case since the formation of its complex with tetraphosphonate cavitands can be monitored through the increase of the luminescence intensity of the pyrene, due to the decrease of exoergonicity of the photoinduced electron transfer process from the pyrene to the methylpyridiniun induced by the formation of the host−guest complex, as previously reported.[12a] As a consequence, to avoid the presence of overlapping signals coming from chromophores of the same nature, we used **2** instead of **3**.

The absorption spectrum of this solution (Figure 4) was the sum of the spectra of the two components, proving that no interaction occurred at this stage among NAPY and **7**. In particular in the 270−300 nm range, the spectrum is dominated by a band typical of the pyrene unit (not shown for clarity), while in the region between 300 and 400 nm both NAPY (prevalently in the 300−345 nm region) and pyrene (prevalently at lower energies) absorb with similar efficiency (violet line in

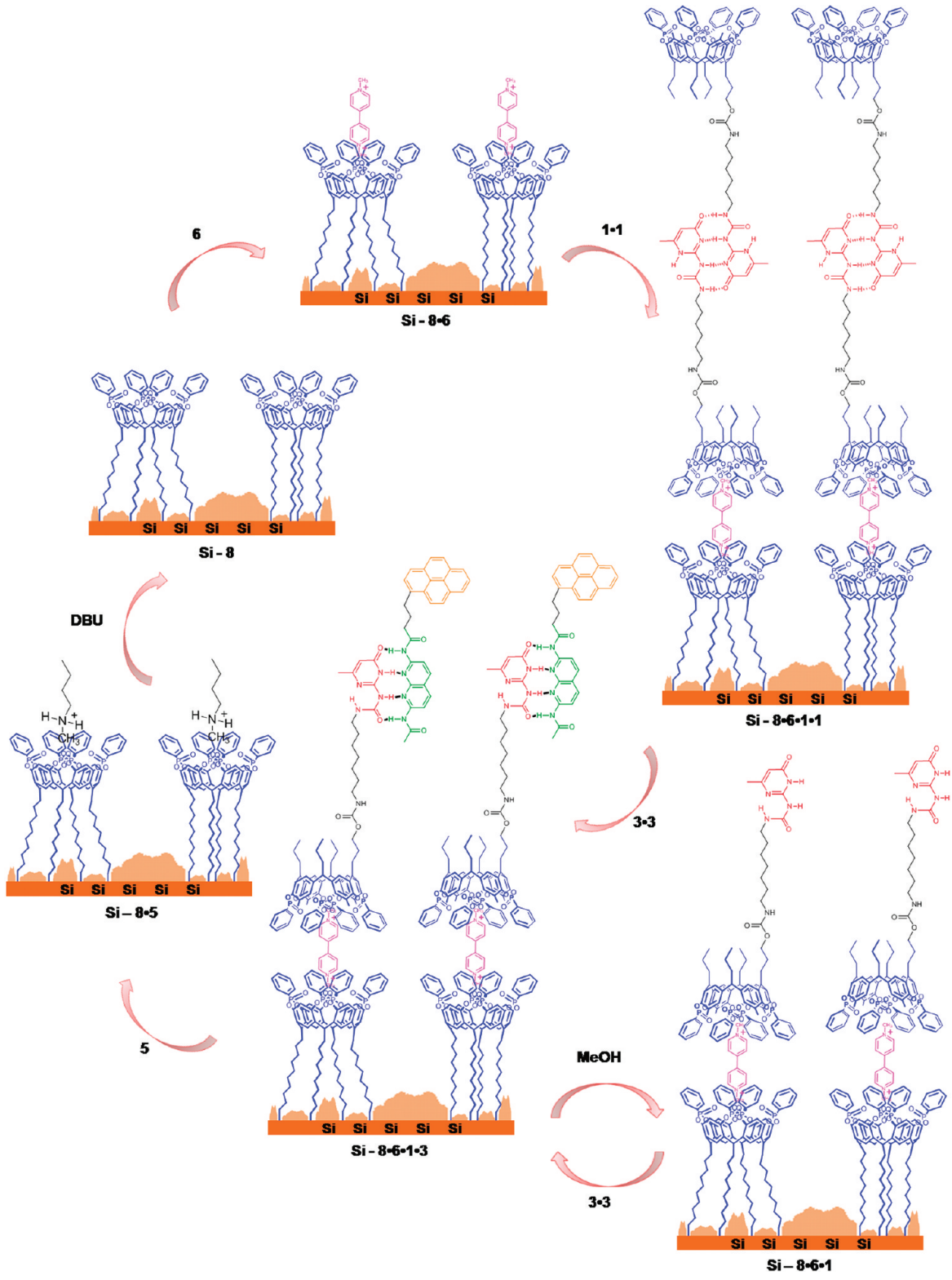

Figure 6. Self-assembly cycle on the Si-surface. The lumps on the Si-wafer indicate SiO_2 growth on the surface after cavitand grafting.

Figure 4). Accordingly, also the fluorescence spectrum (black line in Figure 5a), where the contributions of both NAPY and **7** are present, is the one expected assuming no association and the lack of any energy transfer process among the two species in solution.

The following step in this experiment was the addition of **1**, which, on the contrary, led to noticeable changes in both the absorption and emission spectra. In particular, a slight decrease of the absorbance was observed at 330 and 346 nm, together with an absorbance increase around 355 nm. These changes are those expected from the association of UPY and NAPY, since they were already observed in an analogous experiment performed in the absence of **7** in solution, and particularly the band rising at 355 nm is distinctive for the **1**·**2** complex.

The absorption spectroscopy did not provide, however, any information about the eventual association between the cavitand unit in **1** and the methylpyridinium in **7**, since the absorption spectrum of this host−guest complex is simply the sum of the components spectra.

On the contrary, fluorescence spectroscopy revealed that interesting changes in the luminescence properties of the system occur during the host−guest complex formation. On one hand, after a careful correction of the spectra, it was possible to evidence an increase of the signal in the 380−460 nm region, where the emission of the pyrene unit of **7** rises upon the tail of the emission band of NAPY; this emission increase can be explained by the formation of the host−guest complex between **1** and **7**, as previously explained.[12a] On the other hand, the fluorescence measurements gave further support to the formation of the **1·2** complex: Figure 5a displays the characteristic decrease of emission intensity in the 340−380 nm region that NAPY features when complexed to an UPY unit; the same quenching efficiency was observed in the analogous experiment carried out in the absence of **7**. It is noteworthy that in this case the efficiency of an eventual energy transfer process from NAPY to the pyrene derivative in **7** in the **1·2·7** ensemble is negligible, most probably because of the large separation between these two units; the same energy transfer process is instead quite efficient in **3**, where the same units are connected by a short spacer.

The evidence from both the absorption and the fluorescence spectra are thus in agreement with the formation of the ternary **1·2·7** adduct. To further support this conclusion, we added an equivalent of **5** as hexafluorophosphate salt. A decrease of the fluorescence intensity in the 380−460 nm region was observed (Figure 5b), as expected, because the more competitive ammonium salt can expel the methylpyridinium moiety from the cavity, thus restoring the original, low-fluorescence intensity of the pyrene group in **7**.

It is worth noticing that, as evidenced by NMR spectroscopy for **1·3·5**, the attempt to break the newly formed **1·2·5** host−guest complex by addition of a base able to deprotonate the ammonium salt, reducing its affinity for the cavitand, failed. In this case, in fact, DBU interacted before with the H-bonded network than with the host−guest system, leading to the dissociation of UPY−NAPY units. Therefore, this approach was unfit for closing the assembly/disassembly cycle. Moving the entire protocol on the silicon surface will overcome this problem.

Compexation Studies on Silicon Surface

Cavitand Grafting and XPS Characterization. To perform the complexation studies on the surface summarized in Figure 6, the first step was grafting cavitand **8** on a silicon wafer, via photochemical hydrosilylation on an H-terminated Si(100) surface. The procedure, described in detail in ref 12c, consists in first etching with a 2.5% HF solution to remove the native oxide, followed by surface decoration with cavitand **8** via photochemical hydrosilylation. The hydrogenated Si-wafer was soaked in a degassed 50 mM solution of **8** in mesitylene and irradiated with 254 nm UV radiation, inducing the hydrosilylation of the cavitand terminal double bonds. In this way robust Si−C bonds between the substrate and the organic molecule formed, affording a cavitand-decorated surface, as proved by X-ray photoelectron spectroscopy (XPS) measurements (Table S1, Figure S4, SI), which confirmed the presence of phosphorus on the wafer. Angular resolved XPS experiments on the O 1s band (Figure S3, SI) excluded the possibility of different grafting

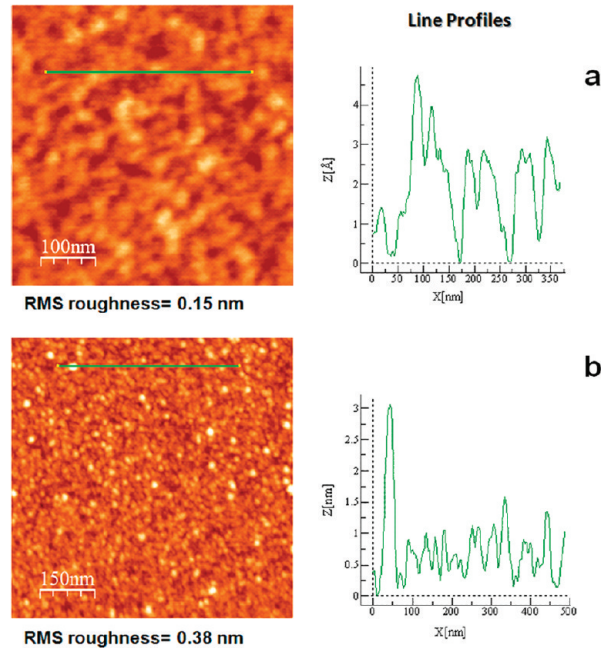

Figure 7. AFM topography image and surface profile for **Si−8** layer (a) and **Si−8·6·1·1** layer (b).

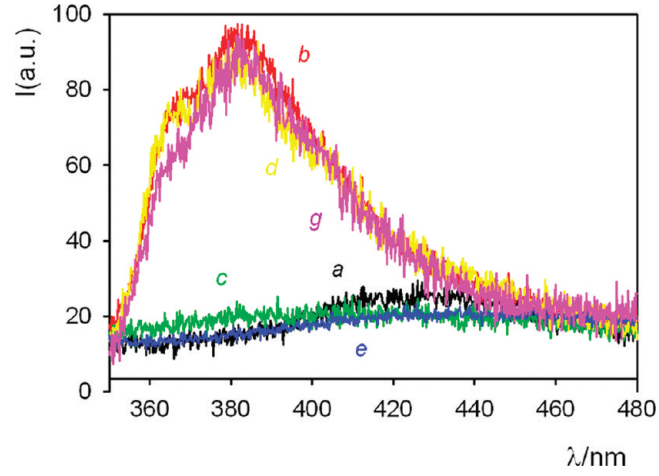

Figure 8. Fluorescent emission spectra of disassembled/reassembled modular components on the Si-surface.

geometries, such as through the phosphonate bridges, since the P═O groups are significantly distant from the surface.[12c] In this case, we chose to prepare a pure cavitand monolayer in order to maximize the amount of receptors on the silicon surface. Under these conditions, the wafer coverage is not complete, leading to oxidation of the residual bare Si-surface with formation of interstitial oxide among cavitands.[23]

AFM. Atomic force microscopy (AFM) was employed to interrogate the topology of the formed layers. The AFM topography image and the surface profile of the starting Si-monolayer are shown in Figure 7a. As expected, under consideration of the vertical resolution limit of the AFM technique, a relatively flat surface was observed, which agrees with the previously proposed scenario.

We then proceeded with a hierarchical construction of a supramolecular structure, exploiting the self-assembly-driven

(23) Condorelli, G. G.; Motta, A.; Favazza, M.; Fragalà, I. L.; Busi, M.; Menozzi, E.; Dalcanale, E.; Cristofolini, L. *Langmuir* **2006**, *22*, 11126–11133.

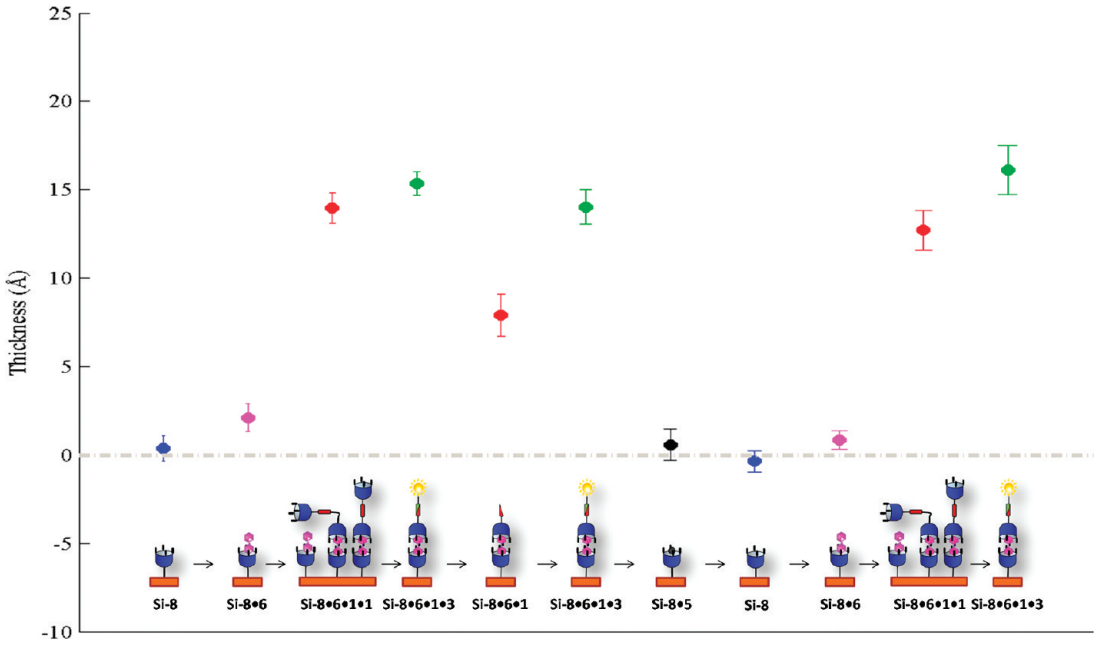

Figure 9. Average thickness of the different self-assembled layers on Si measured by ellipsometry. The **Si−8** layer thickness was set to 0 for clarity.

growth. The cavitand-decorated Si-surface was dipped into a 1 mM solution of methyl viologen **6** in acetonitrile, in order to obtain the guest complexation. After removal of the physisorbed guest by extensive rinsing with CH_3CN and $CHCl_3$, the Si-wafer was exposed to a 1 mM solution of **1·1** homodimer in chloroform. The surface was rinsed again to remove the physisorbed species; then the AFM image of the grown **Si−8·6·1·1** structure was collected.

As shown in Figure 7b, a well-defined profile was traced, featuring peaks of different height, in a range between 1.5 and 3 nm. These data demonstrated the growth of nanometric structures on the surface. In particular, the bigger peaks correspond to the length of the elongated **1·1** dimer linked at the surface due to host−guest interactions between the cavity of **1** and the still free pyridinium moiety of the previously anchored dimethyl viologen. As far as the smaller peaks are concerned, they can be attributed either to a looped structure where the **1·1** dimer is anchored to two adjacent **Si−8·6** units (see Figure S5 in SI) or to a partial bending over the surface of **Si−8·6·1·1** to minimize the surface free energy.[24]

Fluorescence Spectroscopy. In order to follow precisely the next steps and the successive assembly disassembly processes, we turned to fluorescence measurements on the surfaces. The starting point was the fluorescence-silent structure **Si−8·6·1·1** (Figure 6 and Figure 8, trace a, black). Upon exposure to a 1 mM solution of **3·3** homodimer in chloroform, **Si−8·6·1·3** structure formed, according to the exchange mechanism previously reported in solution (Figure 2). As result, a pyrenic unit was anchored on the surface, affording an emission band typical for the monomeric form of pyrene in the recorded surface fluorescence spectrum (Figure 8, trace b, red).

Dipping the **Si−8·6·1·3** wafer in a 8:2 $CHCl_3$/MeOH mixture resulted in the disassembly of unit **3**, as proved by the disappearance of the pyrenic band (Figure 8, trace c, green, and Figure 6). The subsequent treatment with a 1 mM solution of **3·3** homodimer restored the destroyed H-bonded network, as confirmed by the reappearance of the pyrenic peak in the fluorescence spectrum (Figure 8, trace d, yellow, and Figure 6).

Selective host−guest exchange was obtained by simply dipping **Si−8·6·1·3** into a 1 mM solution of butylmethylammonium iodide **5** in chloroform, with the consequent disappearance of the pyrene emission band in the collected spectrum (Figure 8, trace e, blue).

Immersion of **Si−8·5** in a DBU solution restored the initial **Si−8** surface by removing guest **5** (Figure 6, trace f, cyan), ready to repeat the cycle again. The whole assembly cycle is highly reproducible, as shown by the fluorescence spectrum of the **Si−8·6·1·3** reassembled system (Figure 8, trace g, magenta).

Ellipsometry. Another independent way to track the self-assembly process relies on ellipsometry, which provides highly accurate average thickness measurements.[25] The same self-assembly cycle depicted in Figure 6 and tracked by surface fluorescence has been monitored via null ellipsometry at the single wavelength $\lambda = 633$ nm, with an incidence angle of 70°.[26] Inversion of the data (ellipsometric angles Δ and Ψ) to yield the film thickness was performed in the Drude approximation.[27] In this approximation, the angle Ψ is not affected by the film, and its constant value can be used as a check of the overall alignment. The variation $\delta\Delta$ of the phase angle Δ is linearly proportional to the film thickness via a coefficient depending, among other things, on the refractive index of the layer, which is not known exactly in our case because of its composite nature. To get the most reliable estimate of film thickness, the measurements were repeated on a grid of 3×3 or 4×4 points on the surface of the Si-wafer. The average value of those independent measurements and its standard deviations were taken as the best estimate for Δ and Ψ. The error bars in Figure 9 arise from the combination of two factors: spread on the

(24) Chen, T.; Ferris, R.; Zhang, J.; Ducker, R.; Zauscher, S. *Prog. Polym. Sci.* **2010**, *35*, 94–112.
(25) Azzam, R. M. A.; Bashara, N. M. *Ellipsometry and Polarized Light*; North Holland: Amsterdam. 1977.
(26) Harke, M.; Teppner, R.; Schulz, O.; Motschmann, H. *Rev. Sci. Instrum.* **1997**, *68*, 3130–3134.
(27) Tompkins, H. *A User's Guide to Ellipsometry*; Academic Press: Boston, 1993.

measured values and uncertainty in the film refractive index, which is assumed to be in the range $n = 1.45-1.60$, typical for non-mesogenic organic materials. The absorption of the organic components is negligible at $\lambda = 633$ nm.

As a starting point we characterized the initial **Si−8** surface (leftmost blue point in Figure 9), which provides the reference initial thickness of 5.5 nm. This value accounts for the native silicon oxide and the cavitand layer. Given the similarity in the refractive index of silicon oxide ($n = 1.46$) and of the organic layer, it is not possible to discriminate between the two; however the typical value for equilibrium oxide is 2.5 nm,[25] which allows estimating the organic layer thickness at about 3 nm.[28]

Each single self-assembly step was then monitored. The complexation of methyl viologen led to a small but detectable increase of layer thickness. A much larger increase was obtained in the subsequent formation of **Si−8·6·1·1**, quantified at about 1.5 nm. The measured thickness of the layer fully supports the AFM image (Figure 7b), indicating the prevalent formation of 1.5 nm high objects. The **Si−8·6·1·1** structure is flexible enough to bend over the surface whenever possible, in order to minimize the surface free energy.[24] The alternative formation of looped structures (see Figure S5, SI) cannot be excluded *a priori*. The **Si−8·6·1·1** to **Si−8·6·1·3** conversion led only to a tiny thickness variation, as expected for structures of comparable dimensions. The truly remarkable changes were observed in the two orthogonal disassembly modes. Solvent-driven removal of the fluorescent NAPY probe resulted in a 9 Å decrease of layer thickness, fully recovered upon exposure of the wafer to a **3·3** solution. Even more compelling is the guest exchange leading to the **Si−8·5** coverage, substantiated by a 1.4 nm drop in layer thickness. The complexation of **5** does not determine a sizable increase of **Si−8·5** dimensions with respect to the original **Si−8** layer, since the small guest is encased within the cavity. The whole process was repeated to assess its reproducibility. Treatment with DBU restored the initial **Si−8** surface, which underwent complexation to give **Si−8·6.** Exposure of the wafer to a solution of **1·1** brought the layer thickness back to the **Si−8·6·1·1** original value. The same holds for the final conversion of **Si−8·6·1·1** to **Si−8·6·1·3** (rightmost green point in Figure 9).

A bare silicon wafer underwent the same treatment, to exclude physisorption phenomena. Ellipsometry did not evidence any thickness variation at any stage of this control experiment.

Conclusions

In this paper we have introduced a robust and reliable methodology for the self-assembly of complex architectures on silicon. The multistep growth of such supramolecular structures on the surface resulted from the combined use of orthogonal host−guest and H-bonding interactions, embedded in selected modular components. The two interactions are fully compatible in the assembly mode and individually addressable in the disassembly mode, enabling the molecular level control of each step on the surface and their complete reversibility under precise external stimuli. The entire process has been fully tested and characterized in solution and then successfully transferred to the solid state. The transfer of the protocol to the silicon surface requires (i) the covalent grafting of cavitand **8** on a silicon wafer as reactive layer to initiate the building process and (ii) the ditopic methyl viologen **6** for the multistep growth.

The design of the building blocks and of the entire protocol sequence was finalized to allow univocal surface characterization and to achieve complete reversibility. Ellipsometry and fluorescence measurements provided compelling evidence of each step of the self-assembly process on the surface respectively from the topographical and structural point of view. The **Si−8·6·1·1** to **Si−8·6·1·3** conversion allowed the introduction of the pyrene moiety for fluorescence detection, while the **Si−8·6·1·3** to **Si−8·5** guest exchange, followed by basic treatment, reset the starting surface. The problem related to the only nonorthogonal disassembly process in solution, namely, the DBU treatment of **1·3·5**, has been overcome on silicon, where a full cycle has been realized (Figure 6).

This work demonstrated that H-bonding and host−guest interactions can be concurrently employed to realize stimuli-responsive surfaces and complex hybrid organic−inorganic materials.

Acknowledgment. This work was supported by the EC through the ITN Project FINELUMEN (PITN-GA-2008-215399) and the Project BION (ICT-2007-213219). Financial support from INSTM to F.T. is gratefully acknowledged. We acknowledge the Centro Interfacoltà di Misure "G. Casnati" of the University of Parma for the use of NMR and HR ESI-MS facilities, and Prof. G. G. Condorelli of the University of Catania for the preparation and XPS characterizations of the **Si-8** surface. M.M. and L.P. acknowledge the fundamental financial support from Cassa di Risparmio in Bologna and MIUR (PRIN and FIRB). Finally, we are grateful to Prof. J. de Mendoza for helpful discussions and to one referee for suggesting the use of ellipsometry.

Supporting Information Available: Preparation and characterization of compounds **II**, **III**, **IV**, **V**, **1**, and **3**, fluorescence measurements details, XPS atomic composition analysis of HF freshly etched surface, additional ^{1}H NMR spectra, and pure **Si−8** monolayers (Table S1), and picture of the possible arrangements of **1·1** homodimers on the Si-surface (Figure S5). This material is available free of charge via the Internet at http://pubs.acs.org.

JA9099938

(28) This value is higher than expected for the cavitand layer (2.0 nm). The presence of adventitious carbon has been shown to increase the organic layer thickness in silicon wafers. See: Subramanian, V.; Bhattacharya, P. K.; Memon, A. A. *Int. J. Electron.* **1995**, *78*, 519–525.